AIP | Physics of Fluids

Huge reduction in pressure drop of water, glycerol/water mixture, and aqueous solution of polyethylene oxide in high speed flows through micro-orifices

Tomiichi Hasegawa, Akiomi Ushida, and Takatsune Narumi

Citation: Physics of Fluids (1994-present) **21**, 052002 (2009); doi: 10.1063/1.3129592
View online: http://dx.doi.org/10.1063/1.3129592
View Table of Contents: http://scitation.aip.org/content/aip/journal/pof2/21/5?ver=pdfcov
Published by the AIP Publishing

Huge reduction in pressure drop of water, glycerol/water mixture, and aqueous solution of polyethylene oxide in high speed flows through micro-orifices

Tomiichi Hasegawa,[1,a)] Akiomi Ushida,[2] and Takatsune Narumi[1]
[1]*Faculty of Engineering, Niigata University, Niigata 950-2181, Japan*
[2]*Graduate School of Science and Technology, Niigata University, Niigata 950-2181, Japan*

(Received 28 June 2008; accepted 10 April 2009; published online 7 May 2009)

Microfluid mechanics is one of the most exciting research areas in modern fluid mechanics and fluid engineering because of its many potential industrial and biological applications. In the present study, pressure drops (PDs) were measured for water, a 50/50 glycerol/water mixture, and a 0.1% aqueous solution of polyethylene oxide (PEO) 8000 flowing at high velocities through various sizes of micro-orifice. It was found that the measured PD of water and the glycerol/water mixture agrees with the prediction of the Navier–Stokes equation for orifices 100 and 400 μm in diameter, but it is lower for orifices less than 50 μm in diameter. In particular, the measured maximum PD was almost two orders of magnitude lower than the prediction for the 10 and 5 μm diameter orifices. The glycerol/water mixture, possessing a viscosity ten times higher than water, provided nearly the same PDs as water when the reduction was generated. The solution of PEO produced a lower PD than water and the glycerol/water mixture except for the 400 μm diameter orifice. Several factors, including orifice shape, deformation of orifice foil, wall slip, transition, cavitation, and elasticity were considered but the evidence suggests that the reduction in PD may be caused by wall slip or the elasticity induced in a flow of high elongational rate. © *2009 American Institute of Physics*. [DOI: 10.1063/1.3129592]

I. INTRODUCTION

One of the recent attractive research topics in modern fluid mechanics is *microfluid mechanics* because of its many potential industrial and biological applications. There are many papers on flows through microchannels,[1–12] but studies of flows through micro-orifices or short microtubes are not so common.[13–18] The current study is concerned with the pressure drop (PD) in micro-orifice flows.

The total PD Δp_t necessary for a fluid to be forced to flow through a short channel or a deep orifice of length L and diameter D is conventionally divided as

$$\Delta p_t = \Delta p_e + \Delta p_l, \tag{1}$$

where Δp_e is the excess PD which is generated in entrance and exit regions of the channel flow, and Δp_l is the pressure needed for fluids to pass through the channel under fully developed laminar flow conditions (Poiseuille flow). Furthermore, the dimensionless forms of Δp_t, Δp_e, and Δp_l are

$$2\Delta p_t/(\rho V^2) = K_t, \tag{2}$$

$$\frac{2\Delta p_e}{\rho V^2} = 2\alpha, \tag{3}$$

$$\frac{2\Delta p_l}{\rho V^2} = \frac{L}{D}\frac{64}{\mathrm{Re}}, \tag{4}$$

where ρ is the fluid density and V is the mean velocity, and Re is the Reynolds number given by $\rho VD/\mu$, where μ is the viscosity. Furthermore, 2α is conventionally expressed as

$$2\alpha = K + \frac{K'}{\mathrm{Re}}, \tag{5}$$

where K is a constant for high Re and K' is a constant for creeping flows and they are often referred to as the Hagenbach and Couette coefficients, respectively.[19,20]

In principle, the behavior of Newtonian liquids in micro-orifice flows can be theoretically predicted using the Navier–Stokes equation, regardless of the geometric dimensions of the orifice. K' has been found theoretically to be $12\pi/\mathrm{Re}(=37.7/\mathrm{Re})$ for an infinitely thin orifice[21,22] and very close to this value for an orifice of finite thickness.[23] Similar values were obtained numerically by various researchers.[14,15,24] Experimental values of K' for Newtonian flow through orifices of ordinary size (macro-orifices) are also close to the theoretical value: A value of 36.8 was obtained for the flow of glycerol/water mixtures,[25,26] 37.6 for castor oil,[27] and 37 for water.[14] Hence, a value of $K' \approx 37$ can be considered as a universal constant for macro-orifice flow. However, no consistent value of K' has been obtained for micro-orifices experimentally. Hasegawa *et al.*[14] reported a K' value for the 10 μm orifice several times larger than those obtained for larger orifices. Another experiment carried out by Hsiai *et al.*[16] yielded a K' value of 37, which agrees

a)Telephone: +81-25-262-7009. Electronic mail: hasegawa@eng.niigata-u.ac.jp.

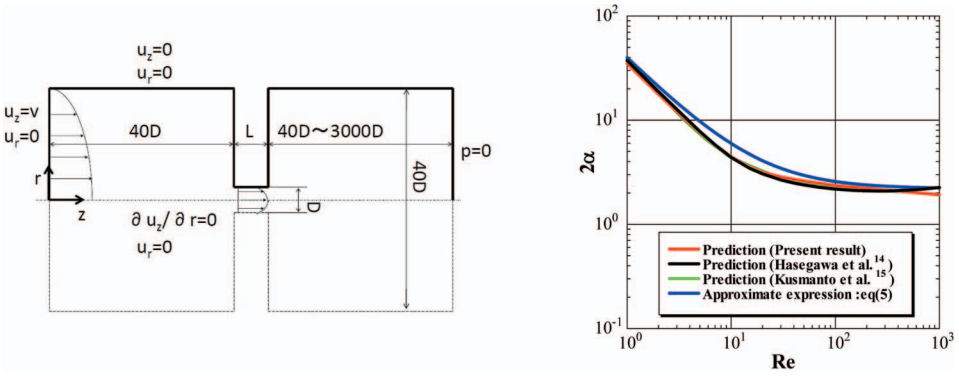

FIG. 1. (Color) (a) Model of channel for the numerical analysis. (b) Result of numerical analysis for 2α vs Re: (red) present result; (black) (Ref. 14); (green) (Ref. 15); (blue) $2\alpha=2.2+37/\mathrm{Re}$.

with the numerical prediction from the Navier–Stokes equation. Kusmanto *et al.*[15] asserted that their numerical result agreed with the experimental data of Hasegawa *et al.*[14] However, their assertion is questionable since they had mistakenly used the experimental excess PD Δp_e for their calculated total PD Δp_t. Experimentally, laminar flow resistance was obtained for short microtubes ranging from 80 to 150 μm in diameter, and the flow resistance was found to be sensitive to the surface roughness of the tube walls.[17] Recently, Oliveira *et al.*[18] presented a detailed numerical study of the flow of a Newtonian fluid through microrheometric devices featuring a sudden contraction expansion and showed that the numerical simulations of the local kinematics and global PD are in good agreement with the experimental results. In addition, the device aspect ratio was shown to have a strong impact on the flow and consequently on the excess PD.

On the other hand, values of K have been determined in the high Re range exclusively using orifices or short tubes larger than 1 mm in diameter. Bond[25] measured Δp_t for solutions of glycerol/water, varying in kinematic viscosity from 10^{-6} to 7×10^{-4} m^2/s, by using an orifice of 1.47 mm in diameter whose ratio of length to diameter was 0.05. The orifice was attached to the end of a pipe of 28.5 mm in inner diameter, through which liquids were made to flow from the inside of the tube to the outside water stored in a large beaker. K was found to be about 2.4 for a range of Re higher than 2000.[25] Johansen[27] carried out experiments measuring Δp_t together with visualization of the flow field through various orifice diameters. He found $K=2.6$ at Re of 10^4. Since this early research, the orifice has been treated exclusively as a flow-metering device by engineers, and today the results are listed in text books or hand books for very high ranges of Re($>$5000): The value of K is known to be highly dependent on entrance geometry such as sharp edges, protrusions, rounded corners, and roughness (see, for example, Refs. 28 and 29). Contraction ratio also influences the characteristics of orifices.[28,30] Interestingly, for short tubes or deep orifices, K takes the highest value 2.7 at the thickness ratio L/D equal to zero and gradually decreases to 1.55 at a ratio of 2.0.[30] For long tubes, the excess PD at the exit amounts to about 40% of that at the entrance.[31] Numerical calculations of orifice flows ranging over large Re are very few, but K about 2.0 has been found.[14,15,24] There seems to be no report on the experimental value of K in micro-orifice flows at high Re.

In the present study, PDs are measured for water, a glycerol/water mixture, and a polymer solution flowing at velocities up to 200 m/s through micro-orifices of diameters ranging from 5 to 400 μm for which the corresponding range of Re becomes the order of 1000 and the strain rate rises to the order of 10^8 1/s. The influence of several factors that may cause a reduction in PD is then discussed.

II. NUMERICAL ANALYSIS

The analysis was carried out using the commercial software package PHOENIX (Concentration Heat and Momentum Lim., U.K.). The finite volume method was adopted for Newtonian fluid flowing through square-edged orifices, in which velocities and pressures were expressed on a staggered grid with a two-dimensional cylindrical coordinate system. Coupling of velocity and pressure was done by the SIMPLEST method. The convective term and viscous term were discretized by the first order upwind difference and by the two order central difference, respectively.

Figure 1(a) shows the model of channel used for the numerical analysis. The diameter of the tube upstream and downstream of the orifice was 40D, the upstream length was 40D, and the downstream length ranged from 40D to 3000D in the z direction according to Re. We confirmed that this region was sufficient for calculation since wider regions gave only negligible differences from the results obtained. The following boundary conditions were adopted: (a) Poiseuille flow exists at the inlet boundary, (b) the pressure and the velocity in the radial direction are zero at the outlet boundary, (c) the radial component of the velocity is zero on the center line, and (d) all velocities are zero at the wall.

Figure 1(b) shows the form of 2α against Re together with the conventional expression of Eq. (5) and the previous numerical results.[14,15] We see the present calculation almost agrees with the previous ones, but gives slightly lower values than Eq. (5).

III. EXPERIMENTAL PROCEDURE AND APPARATUS

Test water was pushed, with the aid of a syringe pump, through a micro-orifice attached to the base of a 25 mm diameter circular channel into water stored in a vessel [Fig. 2(a)]. The pressure differential between the inside of the channel and the water level on the outside was measured at a position 150 mm upstream of the orifice using two pressure

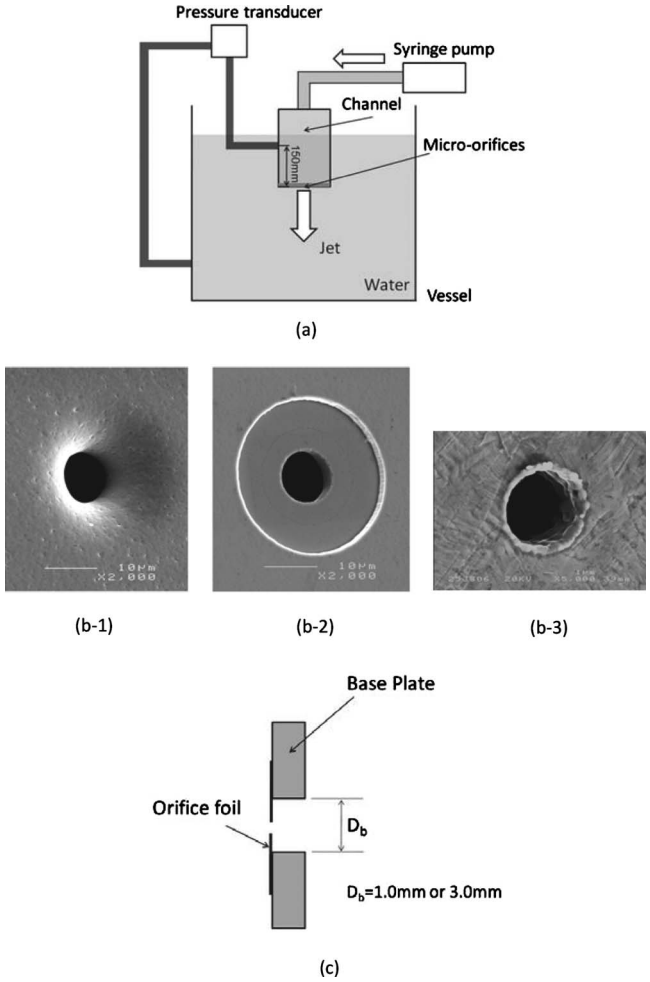

FIG. 2. (a) Schematic of the apparatus for measuring PDs. (b-1) Image of 10 μm diameter nickel orifice, front. (b-2) Image of 10 μm diameter nickel orifice, back. (b-3) Image of 8.5 μm diameter stainless steel orifice. (c) Dimension of base holes.

transducers of different ranges (Nagano Keiki Co., Japan and Tsukasa Sokkenn Co., Japan). In addition, a Bourdon-type pressure gauge (Yamamoto Keiki Instrument Co., Japan) was used for the high pressure range, above 5×10^5 Pa. There was no discernible difference between the pressures measured using different pressure gauges. The flow rate was changed by regulating the output of the syringe pump and measured by reading the dial of the pump. Almost every experiment was conducted by proceeding from low to high Reynolds numbers at the orifice. Several experiments were also conducted proceeding from high to low Reynolds numbers but no difference was found. Calibration was done periodically by ejecting the water in air and determining the mass ejected in a given time. The test water was distilled, deionized to a level of conductance less than 0.5 μS/cm and passed through a filter with pore size 0.20 μm before the experiment. The water temperature was 12 ± 3 °C except in a few cases. Apart from the water, we tested a 50/50 mixture of glycerol and water which has a viscosity 10^{-2} Pa s, ten times higher than the viscosity of water (its temperature was 24 ± 2 °C; this mixture is referred to as G/W mixture hereafter), and an aqueous solution of polyethylene oxide (PEO) of molecular weight 8×10^3 (its weight concentration was 0.1% and the temperature was 12 ± 3 °C). To prevent chemical degradation of molecules, "Sundex C" ($C_6H_{12}N_4$, Meisei Kagaku Co., Japan) was added to the solution with a weight concentration of 0.1%. The PEO solution provided Newtonian viscosity of 10^{-3} Pa s, the same as that of water within the experimental error. In general, PEO solutions are known to show viscoelasticity, but the elasticity of the present PEO solution was too weak to measure because the molecular weight 8×10^3 is relatively low (compared to those of PEOs commonly used). The smallest orifice used was 5 μm and the largest was 400 μm in diameter. Due to the sizes of the orifices, it was difficult to fabricate perfectly circular holes, but the deviation was less than 3%. All orifices used were made of nickel foil and had a thickness of 20 μm, giving a thickness ratio, L/D of between 0.05 and 4 (hereafter L and D indicate the thickness and the diameter of orifice, respectively). An exception was an 8.5 μm diameter orifice of stainless steel (SUS 304) having a thickness of 10 μm and L/D of 1.2. The nickel and stainless steel orifices were made by etching and electrical discharge machining, respectively. The images of the front and back sections of the 10 μm nickel orifice are shown in Figs. 2(b-1) and 2(b-2), and the image of the 8.5 μm stainless steel orifice is shown in Fig. 2(b-3). We observe that the nickel orifices had relatively smooth surfaces, while the stainless steel orifice had a coarse internal surface as well as burrs at the edge. Also, it can be seen for the 10 μm nickel orifice that the front section has a round corner, and the back section has a right angle corner. In most cases, water was made to flow from the front to the back, but the reverse direction of flow was also adopted in several passes in order to examine the effect of the corners on the PD. Table I gives the specifications of the orifices, measurement errors, and experimental uncertainty. The error in K_t is caused by measurement errors of δQ, δD, $\delta(\Delta p_t)$, and $\delta\rho$. Performing standard error analysis, the maximum uncertainties in determining K_t in this experiment were found to be 22% for nickel orifices and 24% for the stainless steel orifice. While these errors seem large, they are sufficiently small compared with the huge reduction in the PD that was observed.

Orifice foils were pasted over a hole of 1 mm in diameter drilled in the base plate [see Fig. 2(c)]. However, some orifice foils were pasted over a hole of 3 mm in diameter so as to examine the effect of foil deformation due to the applied pressure. In addition, an experiment was carried out by ejecting the water in air and determining the mass ejected in a given time in order to measure the flow rate directly rather than by reading the dial of the pump.

IV. EXPERIMENTAL RESULTS

Figure 3 shows examples of the experimental results in the form of Δp_t against V/D, where the data in Figs. 3(a)–3(c) represent both forward (from the front to the back) and backward (from the back to the front) flow results, and there is no discernible difference between the two sets of results. Numerical predictions by the Navier–Stokes equation are also given in the figure with a solid line for water and the

TABLE I. Specification of the orifices used, experimental error, and uncertainty ($\delta\rho<0.1\%$). (Nickel orifices were made by etching and stainless steel orifice by electric discharge machining.)

D (μm)	L (μm)	$L/D(-)$	Material	Hole configuration	Internal surface	$\delta Q/Q$ (%)	$\delta D/D$ (%)	$\delta(\Delta p_t)/\Delta p_t$ (%)	$\delta(2\Delta p_t/\rho V^2)/(2\Delta p_t/\rho V^2)$ (%)
400	20	0.05	Nickel	[a]	Relatively smooth	1	0.1	5	6.4
100	20	0.2	Nickel			1	0.1	5	6.4
50	20	0.4	Nickel			1	1	5	10
25	20	0.8	Nickel			1	1.5	5	12
20	20	1	Nickel			1	1.8	5	13
15	20	1.3	Nickel			1	2	5	14
10	20	2	Nickel			2	2	10	20
5	20	4	Nickel			2	2.5	10	22
8.5	10	1.2	Stainless steel	[b]	Coarse	2	3	10	24

[a]Round corner on the front and right angle corner on the back.
[b]Right angle corners on the front and the back.

PEO solution, and a broken line for the 50/50 G/W mixture. We see in Fig. 3(a) for 100 μm orifice that the experimental Δp_t almost agrees with the prediction for water and the G/W mixture in the whole region examined. However it deviates from the prediction at about 4×10^3 s^{-1} of V/D for the PEO solution and takes a value nearly one order of magnitude lower than that of water at the highest V/D. In Fig. 3(b) for 25 μm orifice, we see that both water and G/W mixture produce an experimental Δp_t consistent with the prediction in the lower range of V/D, but they take smaller values of Δp_t than the prediction in the higher range of V/D. The PEO solution gives Δp_t below its prediction in the region of V/D higher than 10^5 s^{-1}. Figure 3(c) shows the result for a 5 μm orifice, where the all experimental values of Δp_t are well below the prediction. For example, the highest velocity reached for water was about 200 m/s for the 5 μm orifice, and the pressure necessary for such a high velocity is given as 4×10^7 Pa by ρV^2. However, Fig. 3(c) shows that the total pressure required to reach this velocity is only 2.2×10^6 Pa. This result is unexpected when compared to results from orifices of ordinary size. Also, it is interesting and at the same time beyond understanding that both water and the G/W mixture give nearly the same value of Δp_t within the experimental error in cases when the reduction in PD occurs as seen in Figs. 3(b)–3(d), because the 50/50 G/W mixture has ten times higher viscosity than that of water. It is general in fluid mechanics that the higher viscosity produces the higher PD in viscous flows, or otherwise the flow is thought to be under the inertia dominant condition due to its high velocity. [Note that the experimental result that the gradient of log Δp_t against log V/D is nearly constant and almost 45° in Fig. 3(c) seems to mean that this flow is viscous.] Also, Fig. 3(c) contains the data obtained for the 3 mm base hole as well as those for the 1 mm base hole, but little difference in the pressure data obtained for these two base holes was detected. Therefore, together with the data to be shown in Fig. 4(c) for a 10 μm orifice, deformation of orifice foils by pressurization is thought not to be a factor in the decrease in

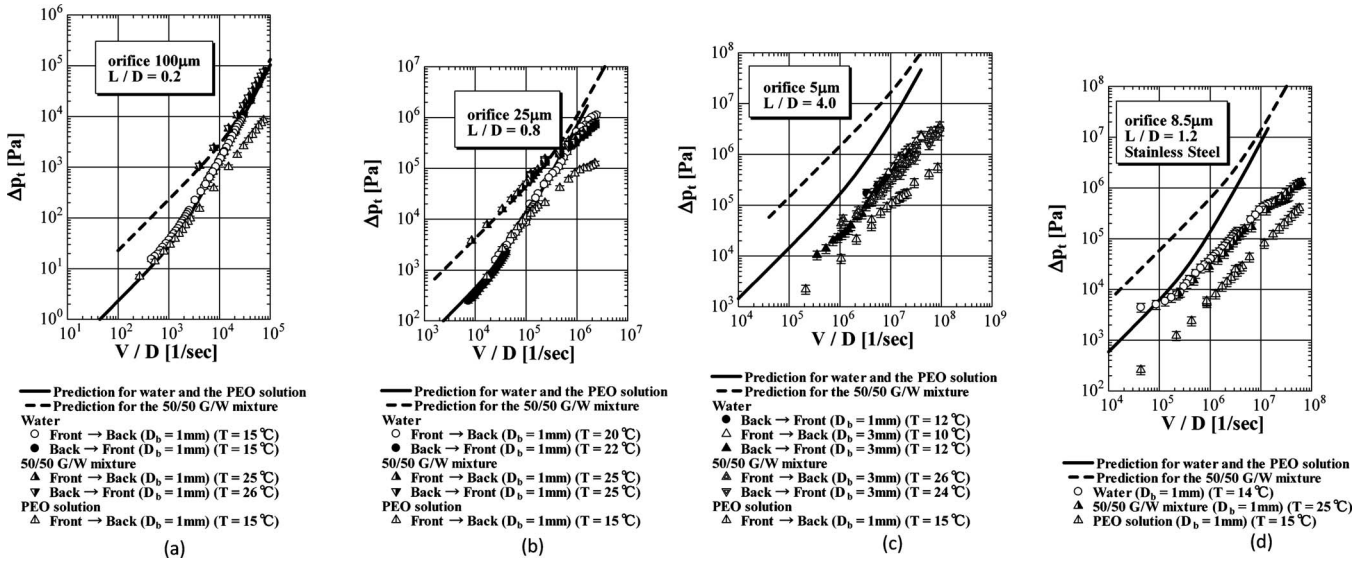

FIG. 3. Examples of the experimental result plotted for Δp_t against V/D: (a) 100 μm orifice, (b) 25 μm orifice, (c) 5 μm orifice, and (d) 8.5 μm orifice. The data except those in (d) contain both the forward (front→back) and backward (back→front) flow results. Numerical predictions by the Navier–Stokes equation are given with a solid line for water and the PEO solution, and a broken line for the 50/50 G/W mixture.

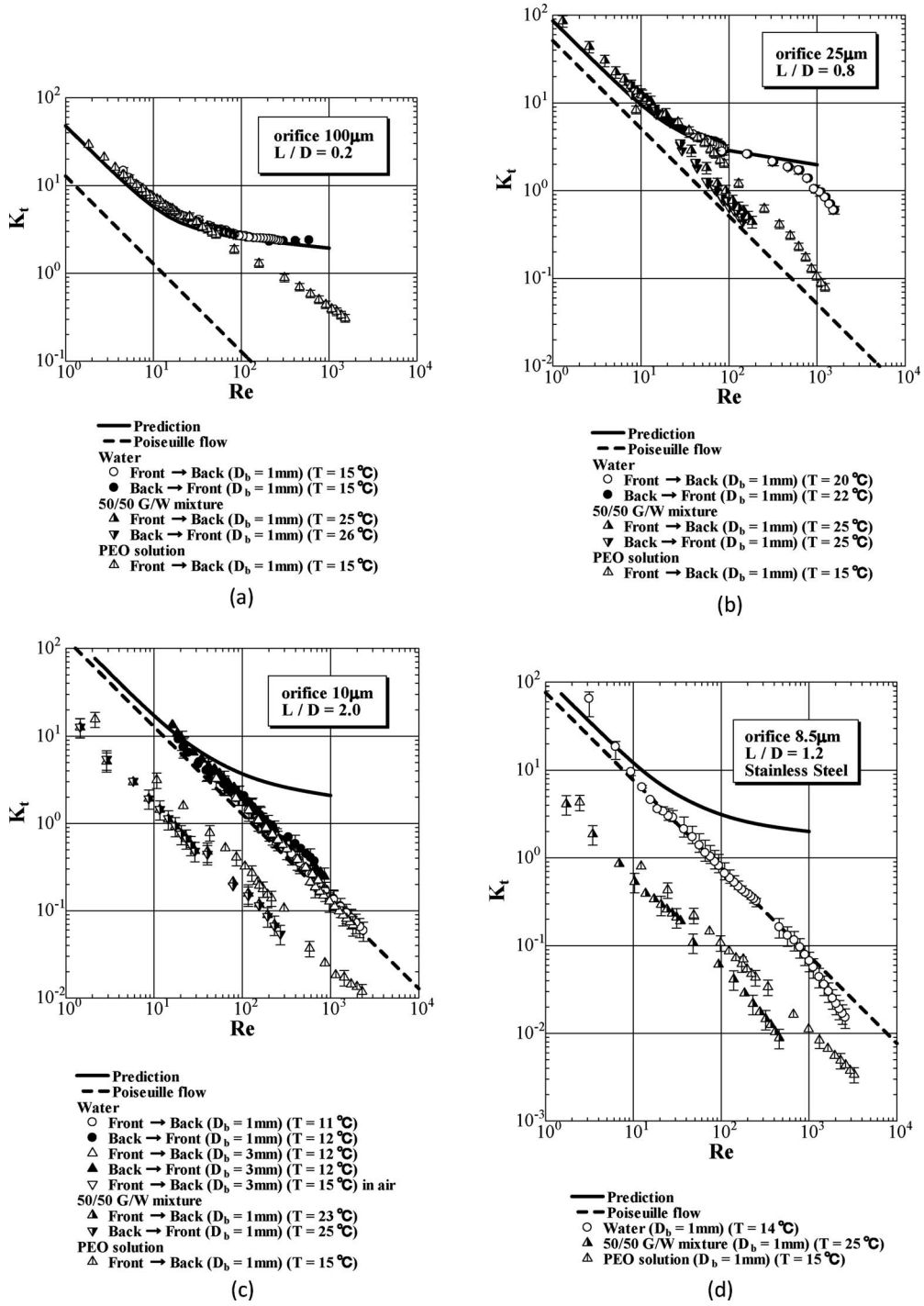

FIG. 4. Dimensionless total PD $K_t(=2\Delta p_t/\rho V^2)$ against Reynolds number $\mathrm{Re}(=\rho VD/\mu)$. Nickel orifices: (a) 100 μm, (b) 25 μm, (c)5μm, and (d) 8.5 μm. The data contain both the forward (front→back) and backward (back→front) flow results. (c) includes the data obtained by ejecting the water in air and determining the mass ejected in a given time. Solid line shows the prediction of the Navier–Stokes equation, and a broken line is the line of Poiseuille flow.

the measured PD. Furthermore, smaller values of Δp_t are seen for the PEO solution in this figure. Δp_t is plotted against V/D for the 8.5 μm stainless steel orifice in Fig. 3(d). It is seen that there is a significant reduction in PD for all the solutions tested similar to that of the 5 μm nickel orifice [Fig. 3(c)] despite the difference in their specifications [see Fig. 2(b) and Table I].

Figures 4(a)–4(d) and EPAPS Document Nos. 1–5 are plots of the total dimensionless PD K_t against Re.[32] Each data point illustrated in the figure is the average of more than three experiments in most cases. Solid and broken lines represent the theoretical prediction using the Navier–Stokes equation and the line for the assumed Poiseuille flow which is given by regarding an orifice as a short tube [see Eq. (4)], respectively. It can be seen that the data fit reasonably well with the prediction for the 400 μm orifice [see EPAPS Document No. 1 (Ref. 32)] for all the liquids tested, and only the PEO solution deviates from the prediction in the range of

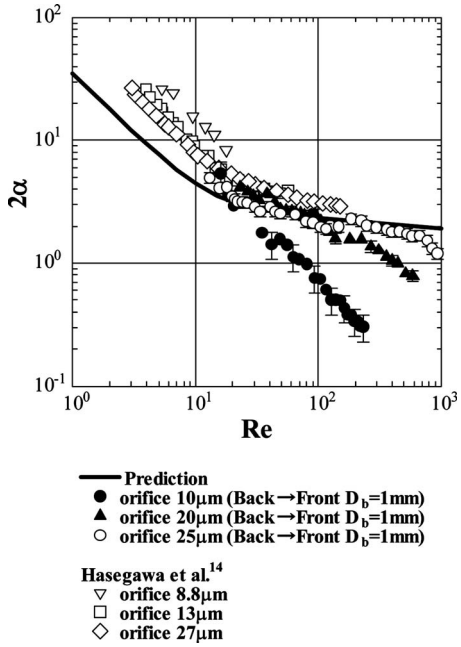

FIG. 5. Dimensionless excess PD $2\alpha(=2\Delta p_e/\rho V^2)$ against Re.

high Re for the 100 μm orifice [Fig. 4(a)]. However, the experimental PDs decrease with the decrease of orifice diameter from 50 to 5 μm [Figs. 4(b)–4(d) and EPAPS Document Nos. 2–5 (Ref. 32)] at high Re even for water and the G/W mixture. In particular, a huge reduction was observed for the 10 μm [Fig. 4(c)], 5 μm orifice [Fig. 6 and EPAPS Document No. 5 (Ref. 32)], and 8.5 orifice [Fig. 4(d)]. We saw that both water and the G/W mixture possessed almost the same value of Δp_t in the region of PD reduction when plotted against V/D, as presented in Figs. 3(b)–3(d), but in Figs. 4(b)–4(d) and EPAPS Document Nos. 2–5,[32] we see that the Re of G/W mixture is ten times lower owing to its high viscosity and hence difference occurs between water and the G/W mixture results. For the PEO solution, larger reduction in K_t is seen for the orifices [Figs. 4(a)–4(d)] except the 400 μm orifice [EPAPS Document No. 1 (Ref. 32)], although the viscosity is almost the same with that of water. Figure 4(c) contains the data obtained by ejecting the water in air. We see a result very similar to the data for ejection into water.

Figure 5 shows the plot of dimensionless excess PD 2α against Re for 10, 20, and 25 μm orifices [2α is negative for the 5 μm orifice as seen in EPAPS Document No. 5 (Ref. 32)] together with the prediction of the Navier–Stokes equation and the previous data of Hasegawa *et al.*[14] It can be seen generally that the Navier–Stokes equation underpredicts the PD in the low Re range, and overpredicts in the high Re range. There is some difference between the present result and the previous one[14] in the range where the excess PD is higher than the prediction. One of the reasons for the disagreement is thought to be in the difference of orifice configuration; the previous orifice was square edged but possessed a bur at the corner,[14] while the present orifice has a round corner in the front and a sharp corner in the back with a rather smooth surface [see Fig. 2(b)]. Also, the disagreement may be due to the difference in precision caused by different experimental purposes: The present experimental apparatus was fabricated for the purpose of clarifying the characteristics of PDs at high velocities, whereas the previous experiment was aimed at measurements at low velocities. Hence, although the present data on 2α show a similar tendency to the previous one, the present experiment is less reliable than the previous one as far as the excess PD at low Re is concerned.

V. DISCUSSION

A. Possible causes of the huge reduction in PD

1. Viscous heating effect

Viscous heating effect may cause a reduction in viscosity or a boundary slip, and it has been argued to be important (mainly in polymer processing) for highly viscous liquids or melts.[33–36] It is also thought to be important in high strain rate flows such as the present micro-orifice flow. The first relevant measure of temperature rise by viscosity may be the temperature increase ΔT_{adiab}, which is given by adiabatic conversion of the PD into heat. That is, $\Delta T_{\text{adiab}}=\Delta p_t/\rho c$, where c is the specific heat.[33] For water $\rho=10^3$ kg/m^3 and $c=4\times10^3$ J/kg K. So, taking 5×10^5 Pa for Δp_t in the present experiment, we obtain $\Delta T_{\text{adiab}}=0.12$ K. This shows a small temperature rise in the present experiment. The same problem can also be treated by the ratio of two dimensionless numbers. One is the Graetz number Gz which is the ratio of the gain rate of internal energy to the heat conduction rate. The other is the Nahme–Griffith number Na which is the ratio of the rate of energy dissipation by viscosity to the heat conduction rate. The ratio of both numbers provides the following relationship: $(\text{Na}/\text{Gz})=(\mu b/\rho c)(V/R)(L/R)$, where $R=D/2$ and b is given by the expression $\mu=\mu_0\exp\{-b(T-T_0)\}$,[33] in which subscript 0 means the quantity at some reference state and $T>T_0$ is assumed here. Now, giving values of $b=0.0255$ K^{-1} for water in the range from 0 to 40 °C, $V=10^2$ m/s, $R=5\times10^{-6}$ m, and $L=2\times10^{-5}$ m, and providing values of μ, ρ, and c for water, we obtain $\text{Na}/\text{Gz}=5.1\times10^{-4}$. This shows again that the heat generation by viscosity is negligible in the present flow.[33]

2. Boundary slip

Many studies, both theoretical and experimental, have been conducted on the flow of liquids near the solid-liquid interface, with particular attention paid to the boundary slip exhibited by Newtonian liquids. Experiments utilizing channel flows of water have produced slip velocities mostly less than 10% of the mean velocity,[37–39] but a few data taken using a lyophobic solid surface showed a slip velocity of 30%–40% of the mean velocity.[40] There are some good review articles regarding recent results on boundary slip in Newtonian fluids.[41,42] Actually, boundary slip is thought to cause reduction in PD, and hence we tried to examine the effect of boundary slip on the PD by numerical simulation. Figure 6 shows an example of the results, where numerical calculation of PDs in the case $L/D=4.0$ was conducted with the slip condition at the wall. The result of the calculation is

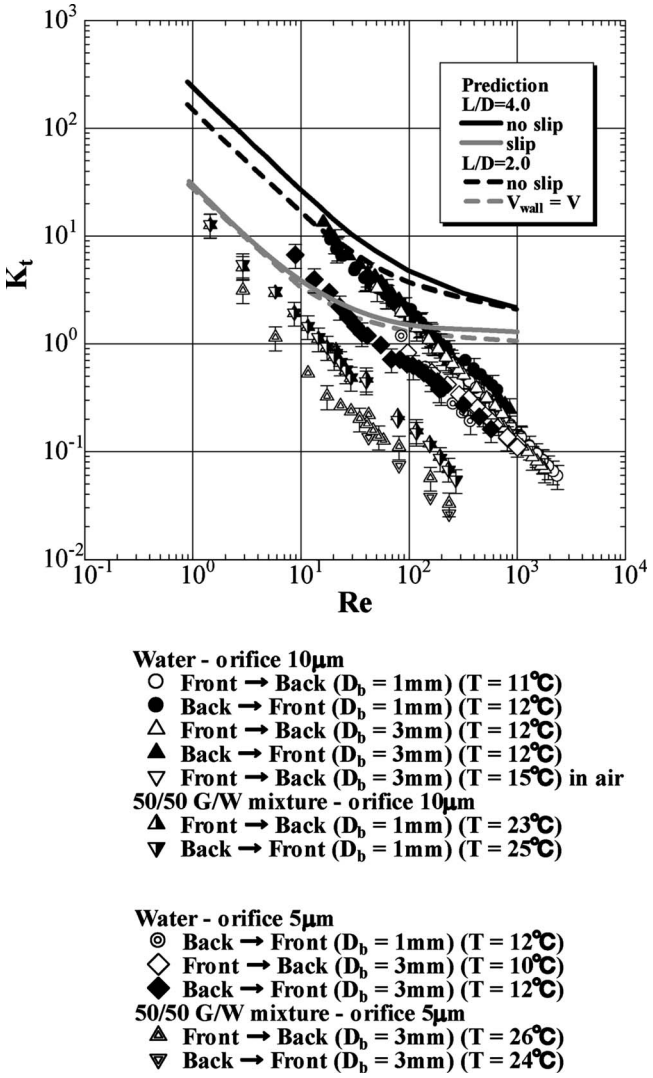

FIG. 6. Influence of wall slip on K_t: no slip at the wall (solid black line for $L/D=4.0$ and broken black line for $L/D=2.0$); permitting slip at the wall (solid gray line for $L/D=4.0$); giving the velocity $V_{wall}(=V)$ as the slip velocity at the orifice wall (broken gray line for $L/D=2.0$).

shown by a gray line together with the result of the no-slip condition (solid black line) and the experimental data. We see that when slipping is allowed, K_t takes a value of about half of that under the no-slip condition at high Re, although this is not enough to explain the reduction effect. Another trial was made for the case $L/D=2.0$ in which the wall velocity at the orifice was assumed to be the mean velocity of the flow through the orifice. The result is also shown in Fig. 6 with a broken gray line. We see that this assumption also gives lower values than the normal calculation (broken black line), but the reduction is insufficient to match the experimental data. However, the trials we made on wall slip are not complete and more exact calculations should be done in the future.

3. Transition

Johansen visualized the flow through a 1.34 cm orifice in a 2.68 cm pipe using the dye injection method.[27] He revealed that vortex ripples or a periodic vortex train appear at the boundary of the jet exiting the orifice for Re between about 200 and 1000, and at Re about 2000 the jet becomes turbulent. Transition in micro-orifices has not been investigated thus far, but several papers describe transition to turbulence in microchannel flows. A few studies report that the transition occurs at smaller Re than the conventional critical Re (early transition),[1,10] whereas another study insists that the transition is similar to the macrochannel case.[11] Figure 4(c) for water seems to indicate the reduction in PD to be caused by delayed transition from laminar to turbulent flow; however, no research to date has mentioned a delayed transition for microchannel flows. In addition, the abrupt increase in PD as generally seen in transition to turbulent flow is not observed [Figs. 4(b)–4(d) and EPAPS Document Nos. 2–5 (Ref. 32)]. Furthermore, the value of K_t is frequently seen to be below that of Poiseuille flow for water [see EPAPS Document No. 5 (Ref. 32)] and the glycerol/water mixture [see Fig. 4(c) for 10 μm orifice, Fig. 4(d) for 8.5 μm orifice, and EPAPS Document No. 5 (Ref. 32) for 5 μm orifice]. It is, therefore, unlikely that the present pressure reduction is caused by delayed transition.

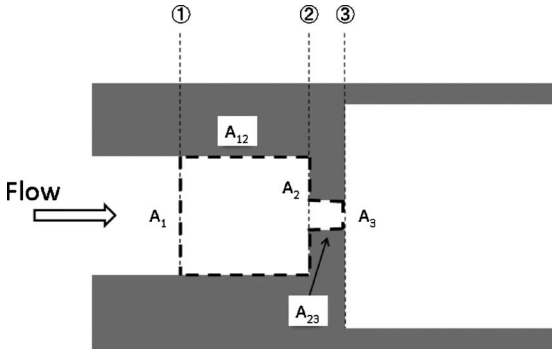

FIG. 7. Control surface including upstream and orifice regions.

4. Cavitations

Cavitations are likely to occur in high speed flows, and have been observed and examined in a microchannel.[43,44] However, cavitation in the channel actually increases the flow resistance leading to a higher PD, instead of lowering it.

5. Fluid elasticity induced at the orifice

The relationship between the PD in orifice flow and rheological properties, such as the elongational and shear viscosities, was derived for the vortex generated flow by Binding[45] and Mackay and co-workers.[46,47] They adopted energetic principles keeping in mind the generation of vortices by the entry flow upstream of the orifice. We begin by applying the law of momentum transport on the orifice flow independent of the occurrence of vortices.

By the momentum balance applied to the control surface enclosing the reservoir from which a jet is issuing through the orifice, as shown in Fig. 7, the following equation is obtained (see Appendix):

$$\beta\rho A_3 V^2 = \Delta p_t A_3 - \tau_w \pi DL + \int_{A_3} \tau_{11} dA. \tag{6}$$

The value of β is slightly greater than unity when Re is higher than 100 for Newtonian fluids. A_3 is the cross sectional area of the orifice at position 3, τ_w is the wall shear stress at the orifice wall, which is equal to $\tau_w = \mu(8V/D)$ if Poiseuille flow is assumed between positions 2 and 3 in Fig. 7, and τ_{11} is the deviatoric normal stress in the z direction (flow direction). Hence, Eq. (6) can be written as

$$\Delta p_t = \beta\rho V^2 + \frac{32\mu V}{D}\frac{L}{D} - \langle NS \rangle, \tag{7}$$

where $\langle NS \rangle = 1/A_3 \int_{A_3} \tau_{11} dA$ is the mean normal stress over the cross section of the orifice exit. According to this equation, Δp_t is reduced by $\langle NS \rangle$. That is, the pressure reduction can be caused by the normal stress generated at the orifice. Here it should be noted that $\langle NS \rangle$ of Newtonian fluids is expressed approximately as $1.8\mu V/D$ by an estimated elongational rate at the orifice in high Reynolds numbers.[48] This becomes the order of 10^5 Pa at the maximum in the present case but it is much smaller than the reduction in PD. Therefore the cause of reduction should be sought for the other, for example, an elasticity induced in very high elongational rates. Aguayo *et al.*[49] carried out numerical calculations using the Oldroyd B model for the 4:1:4 contraction/expansion flow with very small Re($\approx 10^{-2}$) and found a reduced PD. Similar reduction effects were also reported for the same flow condition using FENE-fluid[50] and Oldroyd-B fluid.[51] Also, Hasegawa *et al.*[48] measured the jet thrust of micro-orifice flows and found the reduced jet thrust which suggests the elasticity of water.

VI. CONCLUSION

The PD for water, 50/50 mixture of glycerol and PEO aqueous solution flowing through micro-orifices at high velocities was measured. It was found that the measured PD for water and glycerol/water mixture coincides with the prediction of the Navier–Stokes equation for orifices of 400 and 100 μm diameters, but it is lower than the prediction for orifices less than 50 μm in diameter. The PEO solution produced a lower Δp_t than either water or the glycerol/water mixture except the case of 400 μm orifice. For 10 and 5 μm orifices, the maximum reduction in water and glycerol/water mixture is two orders of magnitude lower than the prediction. Interestingly, both water and the glycerol/water mixture produce almost the same value of Δp_t when the reduction occurs in spite of the increased viscosity in the glycerol/water mixture which is ten times higher than that of water. Such huge reductions in Δp_t were not due to orifice shape or orifice foil deformation. This phenomenon was discussed and shown not to be caused by viscous heating, transition, or cavitations. The evidence suggests that the huge reduction in PD in micro-orifice flows may be caused by wall slip or the elasticity induced in a flow of high elongational rate.

ACKNOWLEDGMENTS

We wish to thank Ryuichi Kayaba, Masanao Takahashi, Shohta Kudou, Hiroteru Haruyama, Dr. Masahiro Karasawa, and Dr. Makoto Ohkawara for technical assistance in carrying out experiments. We also thank Tsunemichi Kawa and Kenji Ogawa for help with the experiment and Professor Tiu Carlos for his fruitful comments and English correction. We are grateful to Professor Masaki Goda, who willingly shared time to discuss the present research with hearty cheers. We would also like to thank Professor Andreas Acrivos and Professor Daniel D. Joseph for useful comments and suggestions.

APPENDIX: DERIVATION OF EQ. (6)

The following equation is obtained by considering balance of momentum at the control surface enclosing the inside of the reservoir from which a jet is ejected, as shown in Fig. 7:

$$\int_{A_3} \rho v^2 dA - \int_{A_1} \rho v^2 dA = -\int_{A_1} T_{11} dA - \int_{A_{12}} \tau_{12} dA + \int_{A_2} T_{11} dA - \int_{A_{23}} \tau_{12} dA + \int_{A_3} T_{11} dA, \tag{A1}$$

where T_{11} is the total normal stress in the $x^1(=z)$ direction (the flow direction). $T_{11} = -p + \tau_{11}$, where τ_{11} is the deviatoric normal stress in the x^1 direction and p is the isotropic pressure. Also, τ_{12} is the shear stress at the control surface, A_1 is the cross sectional area of the upstream tube at position 1, A_3 is the cross sectional area of the orifice at position 3, and A_2 is the wall area at position 2. A_{12} and A_{23} are the wall areas of the larger upstream tube and inside the orifice, respectively (see Fig. 7). There is the following relationship:

$$A_1 = A_2 + A_3, \tag{A2}$$

The following assumptions are thought to be reasonable:

$$\int_{A_1} \rho v^2 dA \ll \int_{A_3} \rho v^2 dA, \tag{A3a}$$

$$\int_{A_1} T_{11} dA \approx -p_1 A_1, \tag{A3b}$$

$$\int_{A_{12}} \tau_{12} dA \approx 0, \tag{A3c}$$

$$\int_{A_2} T_{11} dA \approx -\int_{A_2} p dA, \tag{A3d}$$

$$\int_{A_3} T_{11} dA \approx \int_{A_3} \tau_{11} dA. \tag{A3e}$$

Using these assumptions Eq. (A1) becomes

$$\int_{A_3} \rho v^2 dA = p_1 A_1 - \int_{A_2} p dA - \int_{A_{23}} \tau_{12} dA + \int_{A_3} \tau_{11} dA. \tag{A4}$$

This equation is transformed into the simplified equation

$$\beta \rho A_3 V^2 = \Delta p_t A_3 - \tau_w \pi D L + \int_{A_3} \tau_{11} dA, \tag{A5}$$

where β is a constant to be determined experimentally or theoretically.

[1] G. M. Mala and D. Li, "Flow characteristics of water in microtubes," Int. J. Heat Fluid Flow **20**, 142 (1999).
[2] Q. Weilin, G. M. Mala, and L. Dongqing, "Pressure-driven water flows in trapezoidal silicon microchannels," Int. J. Heat Mass Transfer **43**, 353 (2000).
[3] D. Pfund, D. Rector, A. Shekarriz, A. Popescu, and J. Welty, "Pressure drop measurements in a microchannel," AIChE J. **46**, 1496 (2000).
[4] J. Pfahler, J. Harley, H. Bau, and J. Zemel, "Liquid transport in micron and submicron channels," Sens. Actuators, A **A21–A23**, 431 (1990).
[5] J. Pfahler, J. Harley, H. Bau, and J. Zemel, "Gas and liquid flow in small channels," *Micromechanical Sensors, Actuators, and Systems* (ASME, New York, 1991), DSC-Vol. 32, pp. 49–60.
[6] S.B. Choi, R. F. Barron, and R. O. Warrington, "Fluid flow and heat transfer in microtubes," *Micromechanical Sensors, Actuators, and Systems* (ASME, New York, 1991), DSC-Vol. 32, pp. 123–134.
[7] D. Yu, R. Warrington, R. Barron, and T. Ameel, "An experimental and theoretical investigation of fluid flow and heat transfer in microtubes," *ASME/JSME Thermal Engineering Conference* (ASME, New York, 1995), Vol. 1, pp. 523–530.
[8] X. F. Peng, G. P. Perterson, and B. X. Wang, "Frictional flow characteristics of water flowing through rectangular microchannels," Exp. Heat Transfer **7**, 249 (1994).
[9] P. Wilding, J. Pfahler, H. H. Bau, J. N. Zemel, and L. J. Kricka, "Manipulation and flow of biological fluids in straight channels micromachined in silicon," Clin. Chem. **40**, 43 (1994).
[10] H. Y. Wu and P. Cheng, "Friction factors in smooth trapezoidal silicon microchannels with different aspect ratios," Int. J. Heat Mass Transfer **46**, 2519 (2003).
[11] K. V. Sharp and R. J. Adrian, "Transition from laminar to turbulent flow in liquid filled microtubes," Exp. Fluids **36**, 741 (2004).
[12] M. J. Kohl, S. I. Abdel-Khalik, S. M. Jeter, and D. L. Sadowski, "An experimental investigation of microchannel flow with internal pressure measurements," Int. J. Heat Mass Transfer **48**, 1518 (2005).
[13] C. Mishra and Y. Peles, "Incompressible and compressible flows through rectangular microorifices entrenched in silicon microchannels," J. Microelectromech. Syst. **14**, 1000 (2005).
[14] T. Hasegawa, M. Suganuma, and H. Watanabe, "Anomaly of excess pressure drops of the flow through very small orifices," Phys. Fluids **9**, 1 (1997).
[15] F. Kusmanto, E. L. Jacobsen, and B. A. Finlayson, "Applicability of continuum mechanics to pressure drop in small orifices," Phys. Fluids **16**, 4129 (2004).
[16] T. K. Hsiai, S. K. Cho, J. M. Yang, X. Yang, Y. Tai, and C. Ho, "Pressure drops of water flow through micromachined particle filters," ASME J. Fluids Eng. **124**, 1053 (2002).
[17] D. J. Phares, G. T. Smedlet, and J. Zhou, "Laminar flow resistance in short microtubes," Int. J. Heat Fluid Flow **26**, 506 (2005).
[18] M. S. N. Oliveira, L. E. Rodd, G. H. McKinley, and M. A. Alves, "Simulations of extensional flow in microrheometric devices," Microfluid. Nanofluid. **5**, 809 (2008).
[19] G. Astarita and G. Greco, "Excess pressure drop in laminar flow through sudden contraction," Ind. Eng. Chem. Fundam. **7**, 27 (1968).
[20] N. D. Sylvester and H. Chen, "Excess pressure losses in a sudden contraction," J. Rheol. **29**, 1027 (1985).
[21] R. A. Sampson, "On Stokes current function," Philos. Trans. R. Soc. London, Ser. A **182**, 449 (1891).
[22] R. Roscoe, "The flow of viscous fluids round plane obstacles," Philos. Mag. **440**, 338 (1949).
[23] Z. Dagan, S. Weinbaum, and R. Pfeffer, "An infinite-series solution for the creeping motion through an orifice of finite length," J. Fluid Mech. **115**, 505 (1982).
[24] J. Jeong and S. Choi, "Axisymmetric Stokes flow through a circular orifice in a tube," Phys. Fluids **17**, 053602 (2005).
[25] W. N. Bond, "Viscosity determination by means of orifices and short tubes," Proc. Phys. Soc. London **34**, 139 (1921).
[26] J. Happel and H. Brenner, *Low Reynolds Number Hydrodynamics* (Prentice-Hall, London, 1965), p. 153.
[27] F. C. Johansen, "Flow through pipe orifices at low Reynolds numbers," Proc. R. Soc. London, Ser. A **126**, 231 (1930).
[28] F. M. White, *Fluid Mechanics* (McGraw-Hill, New York, 1979), pp. 356–357.
[29] A. J. Ward-Smith, *Internal Fluid Flow: The Fluid Dynamics of Flow in Pipes and Ducts* (Clarendon, Oxford, 1980), pp. 392–393.
[30] I. E. Idelchik, *Handbook of Hydraulic Resistance* (Hemisphere, Washington, 1986), pp. 174–175.
[31] F. M. White, *Fluid Mechanics* (McGraw-Hill, New York, 1979), p. 357.
[32] See EPAPS Document No. E-PHFLE6-21-009905 for dimensionless total pressure drop against Reynolds number for various orifice sizes. For more information on EPAPS, see http://www.aip.org/pubservs/epaps.html.
[33] J. R. A. Pearson, "Polymer flows dominated by high heat generation and low heat transfer," Polym. Eng. Sci. **18**, 222 (1978).
[34] S. M. Dinh and R. C. Armstrong, "Non-isothermal channel flow of non-Newtonian fluids with viscous heating," AIChE J. **28**, 294 (1982).
[35] Y. T. Shah and J. R. A. Pearson, "Stability of non-Newtonian flow in channels—II. Temperature dependent power-law fluids without heat generation," Chem. Eng. Sci. **29**, 737 (1974).
[36] Y. T. Shah and J. R. A. Pearson, "Stability of non-Newtonian flow in channels—III. Temperature dependent power-law fluids with heat generation," Chem. Eng. Sci. **29**, 1485 (1974).
[37] E. Schnell, "Slippage of water over nonwettable surfaces," J. Appl. Phys. **27**, 1149 (1956).
[38] D. C. Tretheway and C. D. Meinhart, "Apparent fluid slip at hydrophobic microchannel walls," Phys. Fluids **14**, L9 (2002).
[39] C.-H. Choi, K. J. A. Westin, and K. S. Breuer, "Apparent slip flows in hydrophilic and hydrophobic microchannels," Phys. Fluids **15**, 2897 (2003).
[40] N. V. Churaev, V. D. Sobolev, and A. N. Somov, "Slippage of liquids over solid surfaces," J. Colloid Interface Sci. **97**, 574 (1984).
[41] C. Neto, D. R. Evans, E. Bonaccurso, H. J. Butt, and V. S. J. Craig, "Boundary slip in Newtonian liquids: A review of experimental studies," Rep. Prog. Phys. **68**, 2859 (2005).
[42] E. Lauga, M. P. Brenner, and H. A. Stone, "19. Microfluidics: The no-slip boundary condition," in *Springer Handbook of Experimental Fluid Mechanics*, edited by C. Tropea, A. Yarin, and J. Foss (Springer, Heidelberg, 2007), pp. 1219–1240.
[43] C. Mishra and Y. Peles, "Cavitation in flow through a micro-orifice inside a silicon microchannel," Phys. Fluids **17**, 013601 (2005).
[44] C. Mishra and Y. Peles, "Flow visualization of cavitating flows through a rectangular slot micro-orifice ingrained in a microchannel," Phys. Fluids **17**, 113602 (2005).
[45] D. M. Binding, "An approximate analysis for contraction and converging flows," J. Non-Newtonian Fluid Mech. **27**, 173 (1988).
[46] M. E. Mackay and G. Astarita, "Analysis of entry flow to determine elongation flow properties revised," J. Non-Newtonian Fluid Mech. **70**, 219 (1997).
[47] S. A. McGlashan and M. E. Mackay, "Comparison of entry techniques for measuring elongation flow properties," J. Non-Newtonian Fluid Mech. **85**, 213 (1999).
[48] T. Hasegawa, H. Watanabe, T. Sato, T. Watanabe, M. Takahashi, T. Narumi, and T. Carlos, "Anomalous reduction in thrust/reaction of water jets issuing from microapertures," Phys. Fluids **19**, 053102 (2007).
[49] J. P. Aguayo, H. R. Tamaddon-Jahromi, and M. F. Webster, "Excess pressure-drop estimation in contraction and expansion flows for constant shear-viscosity, extension strain-hardening fluids," J. Non-Newtonian Fluid Mech. **153**, 157 (2008).
[50] P. Szabo, J. M. Rallison, and E. J. Hinch, "Start-up of flow of a FENE-fluid through a 4:1:4 contraction in a tube," J. Non-Newtonian Fluid Mech. **72**, 73 (1997).
[51] D. M. Binding, P. M. Phillips, and T. N. Phillips, "Contraction/expansion flows: The pressure drop and related issues," J. Non-Newtonian Fluid Mech. **137**, 31 (2006).